CHAPTER 5

Kinetic Isotope Effects from Hybrid Classical and Quantum Path Integral Computations

JIALI GAO, KIN-YIU WONG, DAN T. MAJOR, ALESSANDRO CEMBRAN, LINGCHUN SONG, YEN-LIN LIN, YAO FAN AND SHUHUA MA

Department of Chemistry, Digital Technology Center and Supercomputer Institute, University of Minnesota, 207 Pleasant Street S.E., Minneapolis, MN 55455-0431, USA

5.1 Introduction

Proton, hydride and hydrogen-atom transfer reactions are ubiquitous in biological processes,[1] and because of their relatively small mass, zero-point energy and quantum tunnelling are significant in determining free-energy reaction barriers.[2,3] The incorporation of nuclear quantum effects (NQE) is also important for reactions involving heavy atoms since one of the most direct experimental assessment of the transition state and the mechanism of a chemical reaction is by measurements of kinetic isotope effects (KIE),[1] which are of quantum-mechanical origin. This is illustrated by the work of Schramm and coworkers,[4] who developed highly potent inhibitors to the enzyme purine nucleoside phosphorylase (PNP) based on the transition-state structure derived from measured KIEs. In principle, Schramm's approach can be applied to other enzymes, but in practice it is often limited by the lack of an adequate model to match computed and experimental KIEs. Therefore, it is of great

RSC Biomolecular Sciences
Quantum Tunnelling in Enzyme-Catalysed Reactions
Edited by Rudolf K. Allemann and Nigel S. Scrutton

Published by the Royal Society of Chemistry, www.rsc.org

interest to develop practical computation methods to estimate KIEs for enzymatic reactions.

The challenge to theory is the difficulty to accurately determine the small difference in free energy of activation due to isotope replacements. This is further exacerbated by the complexity and size of an enzyme system that requires statistical averaging. The computational accuracy demands both an adequate treatment of the potential-energy surface that can properly describe the change of the bond orders of the primary and secondary sites and an efficient sampling procedure that can yield converged properties.[5] In this chapter, we describe an integrated path integral free-energy perturbation and umbrella sampling (PI-FEP/UM) approach in molecular-dynamics simulations, and an analytic, integration-free approach based on Kleinert's variational perturbation theory[6] that can systematically improve the accuracy and avoid numerical convergence problems,[7] to compute KIEs for chemical reactions.[8–10] In addition, we present a mixed molecular-orbital and valence-bond (MOVB) theory[11–14] that combines quantum mechanics with molecular mechanics (QM/MM)[15,16] to represent the potential surface of the reactive system. We show that this coupling of a combined QM-MOVB/MM potential-energy surface to describe the electronic structure with path integral–free energy simulation to model the nuclear quantum effects can yield remarkably accurate KIEs for reactions in solution and in enzymes.

Of course, a variety of methods have been developed to treat NQE for gas-phase reactions (see a recent review[17]). In principle, these techniques can be directly extended to condensed-phase systems; however, the size and complexity of these systems make it intractable computationally. Thus, a main goal is to develop new methods, or to extend gas-phase techniques to condensed phases or biomolecular systems. One method that has been successfully introduced to computational enzymology is the ensemble-averaged variational transition-state theory with QM/MM sampling (EA-VTST-QM/MM),[18,19] which has been applied to a number of enzyme systems.[2,20,21] Both primary and secondary KIEs can be computed using the EA-VTST-QM/MM method and the method includes contributions of multidimensional tunnelling. In another approach, Hammes-Schiffer and coworkers utilised a grid-based hybrid approach to model NQE in hydrogen-transfer reactions by numerically solving the vibrational wavefunction of the transferring hydrogen nucleus.[22] So far, only primary KIEs have been computed by this approach.

The discrete Feynman path integral method[23,24] has been used in a variety of applications since it offers an efficient and general approach for treating nuclear quantum effects in condensed-phase simulations.[25–31] In principle, centroid path integral simulations can be directly used to determine KIEs by carrying out two separate calculations for the heavy and light isotope, respectively, and indeed, this has been the approach in most applications; however, the convergence of the computed free-energy barrier from dynamics simulations is typically not sufficient to ensure the desired accuracy for KIE, especially when heavy isotopes and secondary effects are involved. To this end, we have developed a free-energy perturbation technique[10] by perturbing the atomic mass from light to heavy

isotopes in a bisection path integral sampling scheme,[8,9] and this has tremendously reduced the statistical uncertainty in the computed KIEs.[32]

The integrated path integral–free energy perturbation and umbrella sampling (PI-FEP/UM) method involves two computational steps.[10] First, classical molecular-dynamics simulation is carried out to obtain the potential of mean force along the reaction coordinate for a given reaction. Then, centroid path integral simulations are performed to determine the nuclear quantum effects. The most significant feature of these studies is that classical and quantum simulations are fully separated, making it particularly attractive and efficient for enzymatic reactions. This computational approach has been explored previously in the work of Sprik *et al.*[25] and in the quantised classical path (QCP) method by Warshel and coworkers.[33–35] The special feature in the PI-FEP/UM method is to use a free-energy perturbation scheme to obtain accurate KIEs for chemical reactions, by changing the atomic mass from one isotope into another in path integral sampling.[10]

Discretised path integral simulations often face numerical convergence difficulties, especially in view of the required accuracy is less than a fraction of a tenth of one kilocalorie per mole for computing KIEs. The analytic integration results based on Kleinert's variational perturbation theory does not have this problem, and the perturbation series has been shown to be convergent exponentially and uniformly,[6,36,37] making the second-order perturbation (KP2) sufficiently accurate for chemical applications.[7] We describe an automated, numerical integration-free centroid path integral method[7] for estimating KIEs for proton-transfer reactions to illustrate the computational power for potential applications to enzymatic reactions.

In the following we first summarise the theoretical background, the representation of the potential-energy surface, and the PI-FEP/UM computational details. Then, results and discussion are presented. The paper is concluded with highlights of main findings.

5.2 Theoretical Background

5.2.1 Path Integral Quantum Transition-State Theory

The theoretical framework in the present discussion is path integral quantum transition-state theory (QTST), which yields an expression of the quantum-mechanical rate constant. In the discrete Feynman path integral method, each quantised nucleus is represented by a ring of P quasiparticles called beads, whose coordinates are denoted as $\mathbf{r} = \mathbf{r}_i;\ i = 1, \cdots, P$.[23] The discrete paths are closed with $\mathbf{r}_{P+1} = \mathbf{r}_1$, in which each particle (bead) is connected harmonically with its neighbours, corresponding to the imaginary time slices $\tau_i = (i-1)\hbar\beta/P$. A key concept in QTST is the centroid variable in path integration,[27,38–42] defined as the geometrical centre of the quasiparticles:

$$\bar{\mathbf{r}}^{(n)} = \frac{1}{P}\sum_{i=1}^{P} \mathbf{r}_i^{(n)} \tag{5.1}$$

where the superscript (n) specifies the nth quantised atom. The discretisation parameter P is chosen to be sufficiently large such that the numerical results converge to the quantum limit. In this approach, the quantum-mechanical equilibrium properties are obtained from the classical averages for a fictitious system governed by the effective potential[23]

$$V_{\text{eff}}[\{\mathbf{r}_i^{(n)}\},\mathbf{S}] = \sum_{n=1}^{N} \frac{\pi P}{\beta\lambda_n^2} \sum_{i}^{P} (\mathbf{r}_i^{(n)} - \mathbf{r}_{i+1}^{(n)})^2 + \frac{1}{P}\sum_{i}^{P} U(\mathbf{r}_i^{(1)},\cdots,\mathbf{r}_i^{(N)},\mathbf{S}) \qquad (5.2)$$

where N is the number of quantised atoms, $\mathbf{S}$ represents the coordinates of all classical particles, $U(\mathbf{r}_i^{(1)},\cdots,\mathbf{r}_i^{(N)},\mathbf{S})$ is the potential energy of the system, and $\beta = 1/k_{\text{B}}T$ with k_{B} being Boltzmann's constant and T the temperature. In eqn (5.2), the de Broglie thermal wavelength of atom n with a mass of M_n is given by $\lambda_n = (2\pi\beta\hbar^2/M_n)^{1/2}$. Note that the dynamics generated by the effective potential of eqn (5.2) has no physical significance; it is merely used as a procedure to obtain the correct ensemble of configurations.[23,24]

QTST is derived by writing the rate expression analogous to classical TST, which includes a quantum activation term and a dynamical correction factor,[39,42,43] and the QTST rate constant is given by

$$k_{\text{QTST}} = \frac{1}{2} < |\dot{z}| >_{z^{\neq}} \mathrm{e}^{-\beta w(z^{\neq})} \Big/ \int_{-\infty}^{z^{\neq}} \mathrm{d}z\, \mathrm{e}^{-\beta w(z)} \qquad (5.3)$$

where $w(z)$ is the potential of mean force (PMF) as a function of the centroid reaction coordinate $z[\bar{\mathbf{r}}]$, $z^{\neq}$ is the value of $z[\bar{\mathbf{r}}]$ at the maximum of the PMF, and $< |\dot{z}| >_{z^{\neq}} = (2/\pi\beta M_{\text{eff}})^{1/2}$ is a dynamical frequency factor approximated by the velocity for a free particle of effective mass M_{eff} along the reaction coordinate $z[\bar{\mathbf{r}}]$ direction. The exact rate constant is obtained by multiplying the QTST rate constant by a correction factor or transmission coefficient γ_q:[43]

$$k = \gamma_q \cdot k_{\text{QTST}} \qquad (5.4)$$

Equations (5.3) and (5.4) have identical forms to that of the classical rate constant, but unlike classical variational transition-state theory, there is no variational upper bound in the QTST rate constant because the quantum transmission coefficient γ_{q} may be greater than or less than unity. Equation (5.3) was initially derived with the assumption of a planar dividing surface along a rectilinear reaction coordinate. Messina *et al.* described a generalisation of the dividing surface that may depend both on the centroid coordinates and on its momenta.[42]

There is no practical procedure to compute the quantum transmission coefficient γ_{q} in eqn (5.4). For a model reaction with a parabolic barrier along the reaction coordinate coupled to a bath of harmonic oscillators, the quantum

transmission coefficient is the Grote–Hynes (GH) classical transmission coefficient κ_{GH}.[39,44] Often, the classical γ_q is used to approximate the quantum transmission coefficient; however, there is no correspondence between classical and quantum dynamic trajectories and the effects of tunnelling may greatly affect reaction dynamics near the barrier top.

As in classical TST, the PMF, $w(z)$, can be computed from the equilibrium average without any dynamical information, and it is defined by

$$e^{-\beta[w(z)-w(z_R)]} = e^{-\beta\Delta F(z)} = \frac{\langle\delta(z[\bar{\mathbf{r}}]-z)\rangle}{\langle\delta(z[\bar{\mathbf{r}}]-z_R)\rangle} \tag{5.5}$$

where z_R is the minimum point at the reactant state in the PMF and the ensemble average $\langle\cdots\rangle$ is obtained by the effective potential of eqn (5.2). Equation (5.5) also serves as a definition of the path integral centroid free energy, $\Delta F(z)$, at z relative to that at the reactant state minimum. Note that the inherent nature of quantum mechanics is at odds with a potential of mean force as a function of a finite reaction coordinate. Nevertheless, the reaction coordinate function $z[\bar{\mathbf{r}}]$ can be evaluated from the path centroids $\bar{\mathbf{r}}$,[42–43,45] first recognised by Feynman and Hibbs as the most classical-like variable in quantum statistical mechanics.[23] Studies have shown that the activation free energy in the centroid path integral QTST "captures most of the tunnelling and quantisation effects"; which give rise to deviations from classical TST.[46–49]

It is also useful to rewrite eqn (5.3) in combination with eqn (5.5) as follows

$$k_{QTST} = \frac{1}{\beta h} e^{-\beta\Delta F^{\neq}_{CPI}} \tag{5.6}$$

where the centroid path integral free energy of activation $\Delta F^{\neq}_{CPI}$ is defined by

$$\Delta F^{\neq}_{CPI} = \Delta F(z^{\neq}) - F^{R}_{CPI} \tag{5.7}$$

and

$$F^{R}_{CPI} = -\frac{1}{\beta}\ln\frac{1}{\lambda_{eff}}\int_{-\infty}^{z^{\neq}} dz\, e^{-\beta[\Delta F(z)]} \tag{5.8}$$

F^{R}_{CPI} corresponds to the free energy of the system in the reactant (R) state region relative to the lowest point (z_R), which may be interpreted as the entropic contributions or motions correlating with the progress coordinate z. λ_{eff} is the de Broglie thermal wavelength of the centroid reaction coordinate with an effective mass M_{eff} at the dividing surface, which is determined in the centroid path transition state ensemble.

5.2.2 Centroid Path Integral Simulations

In centroid path integral, the centroid position, $\bar{r}$, is used as the principle variable and the canonical QM partition function of a hybrid quantum and classical system, consisting of one quantised atom for convenience, can be written as follows:[23]

$$Q_P^{\mathrm{qm}} = \frac{1}{\Omega}\int \mathrm{d}\mathbf{S} \int \mathrm{d}\mathbf{s} \left(\frac{P}{\lambda_{\mathrm{M}}^2}\right)^{3P/2} \int \mathrm{d}\mathbf{R} \mathrm{e}^{-\beta V_{\mathrm{eff}}(\{\mathbf{r}\},\mathrm{S})} \tag{5.9}$$

where Ω is the volume element of classical particles, P is the number of quasiparticles, $V_{\mathrm{eff}}(\{\mathbf{r}\},\mathbf{s})$ is the effective potential (eqn (5.2)), $\int d\mathbf{R} = \int d\mathbf{r}_1 \cdots \int d\mathbf{r}_P \delta(\bar{\mathbf{r}} = \mathbf{s})$ in which the delta function $\delta(\bar{\mathbf{r}} = \mathbf{s})$ is introduced for use in later discussion, and the centroid $\bar{\mathbf{r}}$ is defined in eqn (5.1). Importantly, eqn (5.9) can be rewritten exactly as a double average in eqn (5.10), which is the theoretical basis in the simulation approach of Sprik *et al.*, called the hybrid classical and path integral,[25] of Hwang and Warshel, called QCP,[34,35] and later, of Major and Gao, called PI-FEP/UM.[8–10]

$$Q_{P\to\infty}^{\mathrm{qm}} = Q_{\mathrm{cm}} \langle \langle \mathrm{e}^{-\beta \Delta \bar{U}(\bar{\mathrm{r}},\mathbf{S})} \rangle_{\mathrm{FP},\bar{\mathbf{r}}} \rangle_U \tag{5.10}$$

where the average $\langle \cdots \rangle_U$ is a purely classical ensemble average obtained according the potential $U(\bar{\mathbf{r}},\mathbf{S})$ (the potential U in eqn (5.2) with a single centroid position for the quantised particle), the average differential potential is given by

$$\Delta \bar{U}(\bar{\mathbf{r}},\mathbf{S}) = \frac{1}{P}\sum_i^P \{U(\mathbf{r}_i,\mathbf{S}) - U(\bar{\mathbf{r}},\mathbf{S})\} \tag{5.11}$$

and the inner average $\langle \cdots \rangle_{\mathrm{FP},\bar{\mathbf{r}}}$ represents a path-integral free-particle sampling, carried out without the external potential $U(\bar{\mathbf{r}},\mathbf{S})$:[10,34,35]

$$\langle \cdots \rangle_{\mathrm{FP},\bar{\mathbf{r}}} = \frac{\int \mathrm{d}\mathbf{R}\{\cdots\} \mathrm{e}^{-(\pi P/\lambda_{\mathrm{M}}^2)\sum_i^P (\Delta \mathbf{r}_i)^2}}{\int \mathrm{d}\mathbf{R} \mathrm{e}^{-(\pi P/\lambda_{\mathrm{M}}^2)\sum_i^P (\Delta \mathbf{r}_i)^2}} \tag{5.12}$$

where $\Delta \mathbf{r}_i = \mathbf{r}_i - \mathbf{r}_{i+1}$. In eqn (5.10), the factor Q_{cm} is the classical partition function defined in,[23]

$$Q_P^{\mathrm{cm}} = \frac{1}{\Omega}\int \mathrm{d}\mathbf{S} \int \mathrm{d}\mathbf{s}\, \mathrm{e}^{-\beta U(\mathbf{s},\mathbf{S})} \left(\frac{P}{\lambda^2}\right)^{3P/2} \int \mathrm{d}\mathbf{R}\, \mathrm{e}^{-(\pi P/\lambda_{\mathrm{M}}^2)\sum_i^P (\Delta \mathbf{r}_i)^2} \tag{5.13}$$

where we have defined the position of the quantised particle centroid to coincide with the coordinates of the corresponding classical particle $\mathbf{s} = \bar{\mathbf{r}}$.

We note that Warshel and coworkers have exploited this idea, which they called the quantised classical path (QCP) method, to estimate NQE for chemical reactions in solution and catalysed by enzymes.[34,35] In QCP, the classical simulations and quantum corrections are fully separated.[50,51] The expression of eqn (5.10) is particularly useful because the quantum free energy of the system can be obtained first by carrying out classical trajectories according to the classical distribution, $\exp[-\beta U(\bar{\mathbf{r}},\mathbf{S})]$, and then, by determining the quantum contributions through free particle sampling based on the distribution $\exp[-\beta(\pi P/\beta\lambda_{\mathrm{M}}^2)\sum_i^P(\Delta\mathbf{r}_i)^2]$. This double averaging yields the exact path integral centroid density,[10,25,34,35] which can be used to determine the centroid potential of mean force:

$$\mathrm{e}^{-\beta w(\bar{z})} = \mathrm{e}^{-\beta w_{\mathrm{cm}}(z)}\langle\delta(z-\bar{z})\langle\mathrm{e}^{-\beta\Delta\bar{U}(\bar{z}[\mathbf{r}],\mathbf{S})}\rangle_{\mathrm{FP},\bar{z}}\rangle_U \tag{5.14}$$

where $w(\bar{z})$ and $w_{\mathrm{cm}}(z)$ are the centroid quantum-mechanical and the classical-mechanical PMF, respectively, and the average difference potential energy $\Delta\bar{U}(\bar{z}[\mathrm{r}],\mathbf{S})$is given in eqn (5.11).

5.2.3 Kinetic Isotope Effects

We first present two algorithms for estimating KIEs using centroid path integral simulations in the context of QCP[34] or hybrid quantum and classical sampling.[25] Then, we present a third algorithm, making use of Kleinert variational perturbation (KP) theory[6] that determines the centroid potential of the mean force analytically without the need of performing discretised path integral sampling.[7]

5.2.3.1 Sequential Centroid Path Integral and Umbrella Sampling (PI/UM)

Using eqn (5.6), the kinetic isotope effects between a light isotope L and a heavy isotope H can be computed by

$$\mathrm{KIE} = \frac{k^L}{k^H} = \mathrm{e}^{-\beta[\Delta F^L(\bar{z}_L^{\neq})-\Delta F^H(\bar{z}_H^{\neq})]}\mathrm{e}^{-\beta\{F^R_{\mathrm{CPI},L}(\bar{z}_L^R)-F^R_{\mathrm{CPI},H}(\bar{z}_H^R)\}} \tag{5.15}$$

where $\bar{z}_L^{\neq}$, $\bar{z}_H^{\neq}$, $\bar{z}_L^R$, and $\bar{z}_H^R$ are, respectively, the values of the centroid reaction coordinate at the transition state and reactant state minimum for the light and heavy isotopes, and $F^{\mathrm{R}}_{\mathrm{CPI},L}(\bar{z}_L^R)$ and $F^{\mathrm{R}}_{\mathrm{CPI},H}(\bar{z}_H^R)$ are the free energies defined by eqn (5.8) for the two isotopes, respectively, which depend on the effective masses associated with the centroid reaction coordinate at the transition state. Equation (5.15) shows that KIEs may be determined by computing the potentials of mean force separately for the L and H isotopes,[9–10,34,35,52] and this can be achieved by first performing umbrella sampling using classical molecular dynamics and then by performing centroid path integral free-particle sampling with the constraints that the centroids of the quantised particles coincide with

the corresponding positions sampled in the classical trajectory. This is, indeed, what is typically done.[9,34,35,52] However, the statistical fluctuations in the actual simulation for computing the potential of mean force is typically as large as, or even greater than, the isotope effect itself, resulting in poor convergence.[10] To alleviate this difficulty, in refs 9 and 10, we have introduced a procedure such that the discretised beads positions for the heavy and light atoms are obtained from exactly the same sampling sequence. Thus, the heavy and light path integral beads distributions differ only by their relative spread from the centroid position, which is determined by the corresponding de Broglie wavelength.

To enhance convergence in these centroid path integral simulations, we have developed a bisection sampling technique for a ring of beads, called BQCP, by extending the original approach of Ceperley for free particle sampling in which the initial and final beads are not connected.[53,54] In our implementation, we first make the bisection sampling as originally proposed by Ceperley,[53,54] enforcing the first and last beads to be identical to enclose the polymer ring.[8,9] Then, we make rigid-body translation of the centroid position of the new beads configuration to coincide with the target (classical) coordinate. Since the free-particle distribution is known exactly at a given temperature, each ring-bead distribution is generated according to this distribution and thus 100% accepted.[54] Furthermore, in this construction, each new configuration is created independently, starting from a single initial bead position, allowing the new configuration to move into a completely different region of configurational space. This latter point is especially important in achieving convergence by avoiding being trapped in a local region of the classical potential in the path integral sampling. The BQCP method has been thoroughly tested[8,9] and applied to several condensed-phase systems.[9–10,55,56]

5.2.3.2 *The PI-FEP/UM Method*

The second algorithm is to obtain the ratio of the quantum partition functions (eqn (5.10)) for two different isotopes directly through free-energy perturbation (FEP) theory by perturbing the mass from the light isotope to the heavy isotope.[10] In other words, only one simulation of a given isotopic reaction is performed, while the ratio of the partition function, *i.e.* the KIE, to a different isotopic reaction, is obtained by FEP within this simulation. This is in contrast to algorithem 1, in which two separate simulations are performed, and this difference results in a major improvement in computation accuracy for KIE calculations.[10,32]

Specifically, eqn (5.15) for computing kinetic isotope effect is rewritten in terms of the ratio of the partial partition functions at the centroid reactant and transition state and is given by:

$$\mathrm{KIE} = \frac{k^L}{k^H} = \left[\frac{Q^L_{\mathrm{qm}}(\bar{z}^{\neq}_L)}{Q^H_{\mathrm{qm}}(\bar{z}^{\neq}_H)}\right]\left[\frac{Q^H_{\mathrm{qm}}(\bar{z}^R_H)}{Q^L_{\mathrm{qm}}(\bar{z}^R_L)}\right] \mathrm{e}^{-\beta\{F^R_{\mathrm{CPI},L}(\bar{z}^R_L)-F^R_{\mathrm{CPI},H}(\bar{z}^R_H)\}} \tag{5.16}$$

where the ratio of the partition function can be written as follows:

$$\frac{Q_{\mathrm{qm}}^{H}(\bar{z})}{Q_{\mathrm{qm}}^{L}(\bar{z})}=\frac{\langle\delta(z-\bar{z})\langle \mathrm{e}^{-\frac{\beta}{P}\sum_i \Delta U_i^{L\to H}}\mathrm{e}^{-\beta\Delta\bar{U}_L}\rangle_{\mathrm{FP},L}\rangle_U}{\langle\delta(z-\bar{z})\mathrm{e}^{-\beta[F_L(\bar{z},\mathbf{S})-F_{FP}^{o}]}\rangle_U} \tag{5.17}$$

where the subscripts L specifies that the ensemble averages are done using the light isotope, $\Delta\bar{U}_L$ is defined by eqn (5.12), $F_{\mathrm{FP}}^{\mathrm{o}}$ is the free energy of the free particle reference state for the quantised particles,[23] and $\Delta U_i^{L\to H}=U(\mathbf{r}_{i,H})-U(\mathbf{r}_{i,L})$ represents the difference in "classical" potential energy at the heavy and light bead positions $\mathbf{r}_{i,H}$ and $\mathbf{r}_{i,L}$. In the bisection sampling scheme, the perturbed heavy isotope positions are related to the lighter ones by

$$\frac{\mathbf{r}_{i,L}}{\mathbf{r}_{i,H}}=\frac{\lambda_{M_L}\theta_i}{\lambda_{M_H}\theta_i}=\sqrt{\frac{M_H}{M_L}};\quad i=1,2,\cdots,\mathrm{P} \tag{5.18}$$

where $\mathbf{r}_{i,L}$ and $\mathbf{r}_{i,H}$ are the coordinates for bead i of the corresponding light and heavy isotopes, λ_{M_L} and $\lambda_{M_H}$are isotopic masses for the light and heavy nuclei, and θ_i is the position vector in the bisection sampling scheme that depends on the previous sequence of directions and has been fully described in ref. 8. Equation (5.18) indicates that the position vectors for the corresponding heavy and light isotope beads in the path integral simulation are identical, thereby, resulting in the relationship that bead positions are solely determined by the ratio of the square roots of masses.

In eqn (5.17), we obtain the free-energy (inner average) difference between the heavy and light isotopes by carrying out the bisection path integral sampling with the light atom and then perturbing the heavy isotope positions according to eqn (5.18). Then, the free-energy difference between the light and heavy isotope ensembles is weighted by a Boltzmann factor for each quantised configuration.

5.2.3.3 Kleinert's Variational Perturbation (KP) Theory

The canonical partition function Q_{QM} for a quantised particle in the bath of classical solvent can be written in terms of the effective centroid potential w, as a classical configuration integral:

$$Q_{\mathrm{P}}^{\mathrm{qm}}=\sqrt{\frac{Mk_{\mathrm{B}}T}{2\pi\hbar^2}}\int_{-\infty}^{\infty}\mathrm{e}^{-\beta w(\bar{\mathbf{r}})}\mathrm{d}\bar{\mathbf{r}} \tag{5.19}$$

where M is the mass of the quantised particle, $\hbar$ is Planck's constant divided by 2π. In the 1980s, three groups proposed a variational method,[39,57,58] known as the Feynman and Kleinert (FK) variational method that yields an upper bound of $w(\bar{\mathbf{r}})$ and has been successfully used in a variety of applications.[59–62] Kleinert later showed that the FK approach in fact is just the first-order approximation to a general variation perturbation theory,[6,36] and the new Kleinert perturbation theory (KP) has been shown in several model systems to have very attractive features, including exponentially and uniformly convergent. For

example, the electronic ground-state energy of a hydrogen atom converges at accuracies of 85%, 95% and 98% in the first three orders of KP expansion. The KP theory does not suffer from the numerical convergence issues in discretised path integral simulations; however, it has so far only been applied to a few limited model cases beyond the first-order approximation, *i.e.* the Feynman–Kleinert approach.

We have shown recently that the KP theory can be adopted in chemical applications to determine KIEs for chemical reactions, and because of its fast convergence the second-order perturbation, denoted by KP2, can yield excellent results for a series of proton-transfer reactions.[7] We briefly summarise the key elements of our theoretical development based on the Kleinert variational perturbation theory.

The nth-order KP approximation $W_{\Omega}^{n}(\bar{\mathbf{r}})$ to the centroid potential $w(\bar{\mathbf{r}})$ is given by

$$-\beta W_{\Omega}^{n}(\bar{\mathbf{r}}) = \ln Q_{\Omega}(\bar{\mathbf{r}}) - \frac{1}{\hbar}\left\langle V_p^{\bar{\mathbf{r}}}[\mathbf{r}(\tau_1)]\right\rangle_{\Omega,c}^{\bar{\mathbf{r}}} + \frac{1}{2!\hbar^2}\left\langle V_p^{\bar{\mathbf{r}}}[\mathbf{r}(\tau_1)]\, V_p^{\bar{\mathbf{r}}}[\mathbf{r}(\tau_2)]\right\rangle_{\Omega,c}^{\bar{\mathbf{r}}} + \cdots + \frac{(-1)^n}{n!\hbar^n}\left\langle \prod_{k=1}^{n} V_p^{\bar{\mathbf{r}}}[\mathbf{r}(\tau_k)]\right\rangle_{\Omega,c}^{\bar{\mathbf{r}}} \tag{5.20}$$

where the angular frequency Ω is a variational parameter, which is introduced to define the perturbation potential $V_p^{\bar{\mathbf{r}}}[\mathbf{r}] = U(\mathbf{r}, S) - U_{\Omega}^{\bar{\mathbf{r}}}(\mathbf{r})$ about the reference state at $\bar{\mathbf{r}}$ with the harmonic potential $U_{\Omega}^{\bar{\mathbf{r}}}(\mathbf{r}) = (M/2)\Omega^2(\mathbf{r} - \bar{\mathbf{r}})^2$. The local quantum partition function of the harmonic reference state $Q_{\Omega}(\bar{\mathbf{r}})$ is given as follows:

$$Q_{\Omega}(\bar{\mathbf{r}}) = \frac{\beta\hbar\Omega(\bar{\mathbf{r}})/2}{\sinh(\beta\hbar\Omega(\bar{\mathbf{r}})/2)} \tag{5.21}$$

The remaining terms in eqn (5.20) are the nth-order corrections to approximate the real system, in which the expectation value $\langle\cdots\rangle_{\Omega,c}^{\bar{\mathbf{r}}}$ is called the cumulant. The cumulants can be written in terms of the standard expectation value $\langle\cdots\rangle_{\Omega}^{\bar{\mathbf{r}}}$ by cumulant expansion. Kleinert and coworkers derived the expression for the expectation value of a function in terms of Gaussian smearing convolution integrals:[6]

$$\left\langle \prod_{k=1}^{n} F[\mathbf{r}_k(\tau_k)]\right\rangle_{\Omega}^{\bar{\mathbf{r}}} = \frac{\prod_{j=1}^{n}\int_0^{\beta\hbar} \mathrm{d}\tau_j \prod_{k=1}^{n}\int_{-\infty}^{\infty} \mathrm{d}\mathbf{r}_k F(\mathbf{r}_k(\tau_k))}{\{(2\pi)^n \mathrm{Det}[a^2_{\tau_k\tau_{k'}}(\Omega)]\}^{3/2}} \times \exp\left\{-\frac{1}{2}\sum_{k'=1}^{n}\sum_{k=1}^{n}(\mathbf{r}_k - \bar{\mathbf{r}})\,.\,a^{-2}_{\tau_k\tau_{k'}}(\Omega)(\mathbf{r}_{k'} - \bar{\mathbf{r}})\right\} \tag{5.22}$$

where $\mathrm{Det}[a^2_{\tau_k\tau_{k'}}(\Omega)]$ is the determinant of the $n \times n$ matrix consisting of the Gaussian width $a^2_{\tau_k\tau_{k'}}(\Omega)$, $a^{-2}_{\tau_k\tau_{k'}}(\Omega)$ is an element of the inverse matrix of the Gaussian width, which is given by

$$a^2_{\tau_k\tau_{k'}}(\Omega) = \frac{1}{\beta M\Omega^2}\left\{\frac{\beta\hbar\Omega\cosh[(|\tau_k - \tau_{k'}| - \beta\hbar/2)\Omega]}{2\sinh[\beta\hbar\Omega/2]} - 1\right\} \tag{5.23}$$

As n tends to infinity, $W^n_\Omega(\bar{\mathbf{r}})$ becomes independent of the variational parameter Ω. At a given order of the KP theory, the optimal frequency is given by the least dependence of $W^n_\Omega(\bar{\mathbf{r}})$ on Ω, which is the solution to the equation of the lowest-order derivative of $W^n_\Omega(\bar{\mathbf{r}})$ setting to zero.[6] Thus, a self-consistent iterative procedure is carried out. Given an initial trial of Ω, the corresponding Gaussian widths are determined using eqn (5.23), with which a new $W^n_\Omega(\bar{\mathbf{r}})$ is obtained. This is then used to obtain a further value of Ω until it is converged.[7]

An especially attractive feature of eqn (5.20) is that if the real system potential U is expressed as a series of polynomials or Gaussian functions, analytic expressions of eqn (5.18) can be obtained,[7] making the computation extremely efficient because there is no need to perform the time-consuming Monte Carlo or molecular dynamics sampling of the path integrals. If the real potential is expanded to the mth-order polynomial and the KP theory is terminated at the nth order (eqn (5.20)), we denoted our results as KPn/Pm.

If the number of quantised particles is N, the angular frequency variational variable is a $3N\times3N$ matrix, and this coupled with the $2n$-dimension integrals in eqn (5.22) makes the use of KP theory rather laborious and has been a major factor limiting its applications beyond the KP1 level, the original FK approach. To render the KP theory feasible for many-body systems with N nuclei for a given configuration $\{\bar{\mathbf{r}}_i; i = 1, \cdots, N\}$, we make use of instantaneous normal mode (INM) coordinates $\{q(\bar{\mathbf{r}}_i; i = 1, \cdots, N)\}^{3N}$ and assume their motions can be decoupled. Thus, system potential $U(\{\mathbf{r}\},\boldsymbol{S})$ can be expanded in terms of the INM coordinates at $\{\bar{\mathbf{r}}_i; i = 1, \cdots, N\}$, and hence, the multidimensional potential is effectively reduced to $3N$ one-dimensional potentials along each normal coordinate. This approximation is particularly suited for the KP theory because of the exponentially decaying property of the Gaussian convolution integrations in eqn (5.22). With the INM approximation, the total effective centroid potential for N-quantised nuclei can be simplified as:

$$W^n_\Omega(\{\bar{\mathbf{r}}_i\}^{3N}) \approx U(\{\bar{\mathbf{r}}_i\}^{3N}, \boldsymbol{S}) + \sum_{i=1}^{3N} W^n_{\Omega_i}(\{q_i\}^{3N}, \boldsymbol{S}) \tag{5.24}$$

where $W^n_{\Omega_i}(\{q_i\}^{3N}, \boldsymbol{S})$ is the centroid potential for normal mode i of the quantised system in the classical bath coordinates of the remainder of the system. Although the INM approximation sacrifices some accuracy, in return, it allows analyses of quantum-mechanical vibration and tunnelling and their separate contributions to the total quantum effects. Note that positive and

negative values of $W^{n}_{\Omega_i}(\{q_i\}^{3N}, \boldsymbol{S})$ in eqn (5.24) raise (vibration) and lower (tunnelling) the classical potential $U(\{\bar{\mathbf{r}}_i\}^{3N}, \boldsymbol{S})$, respectively.

5.3 Potential-Energy Surface

Almost all enzyme reactions can be well described by the Born–Oppenheimer approximation, in which the sum of the electronic energy and the nuclear repulsion provides a potential-energy function, or potential-energy surface (PES), governing the interatomic motions. Therefore, the molecular modelling problem breaks into two parts: the PES and the dynamics simulations.

The potential-energy function describes the energetic changes as a function of the variations in atomic coordinates, including thermal fluctuations and rearrangements of the chemical bonds. The accuracy of the potential-energy function used to carry out molecular-dynamics simulations directly affects the reliability of the computed $\Delta F^{\neq}_{\mathrm{TST}}$ and its nuclear quantum correction.[5,20] The accuracy can be achieved by the use of analytical functions fitted to reproduce key energetic, structural, and force constant data, from either experiments or high-level *ab initio* calculations. Molecular-mechanical (MM) potentials or force fields,[63,64] however, are not general for chemical reactions, and it requires reparameterisation of the empirical parameters for every new reaction, which severely limits its applicability. More importantly, often, little information is available in regions of the PES other than the stationary reactant and product states and the saddle point (transition state). On the other hand, combined quantum-mechanical and molecular-mechanical (QM/MM) potentials offer the advantages of both computational efficiency and accuracy for all regions of the PES.[65,66]

5.3.1 Combined QM/MM Potentials

In combined QM/MM potentials, the system is divided into a QM region and an MM region.[12,15,16,65,67–70,] The QM region typically includes atoms that are directly involved in the chemical step and they are treated explicitly by a quantum-mechanical electronic-structure method, whereas the MM region consists of the rest of the system and is approximated by an MM force field. The method of combining QM with MM was first developed by Warshel and Karplus for the treatment of conjugated polyenes with QM and the framework with a force field,[15] and it was subsequently applied to an enzyme by Warshel and Levitt in which electrostatic interactions between QM and MM were introduced.[16] The remarkable applicability of this approach that it enjoys today was in fact not appreciated until more than a decade later when molecular dynamics and Monte Carlos simulations using combined QM/MM potentials began to emerge.[65,68,71] The QM/MM potential is given by:[66,67]

$$U_{\mathrm{tot}} = \langle \Psi(S) | H^{\mathrm{o}}_{\mathrm{qm}}(S) + H_{\mathrm{qm/mm}}(S) | \Psi(S) \rangle + U_{\mathrm{mm}} \qquad (5.25)$$

where $H^{\mathrm{o}}_{\mathrm{qm}}(S)$ is the Hamiltonian of the QM-subsystem (the substrate and key amino-acid residues) in the gas phase, U_{mm} is the classical (MM) potential

energy of the remainder of the system, $H_{qm/mm}(S)$ is the QM/MM interaction Hamiltonian between the two regions, and $\Psi(S)$ is the molecular wavefunction of the QM-subsystem optimised for $H^{o}_{qm}(S) + H_{qm/mm}(S)$.

We have found that it is most convenient to rewrite eqn (5.25) as follows:[65,68]

$$U_{tot} = E^{o}_{qm}(S) + \Delta E_{qm/mm}(S) + U_{mm} \tag{5.26}$$

where $E^{o}_{qm}(S)$ is the energy of an isolated QM subsystem in the gas phase,

$$E^{o}_{qm}(S) = \langle \Psi^{o}(S) | H^{o}_{qm}(S) | \Psi^{o}(S) \rangle \tag{5.27}$$

In eqn (5.26), $\Delta E_{qm/mm}(S)$ is the interaction energy between the QM and MM regions, corresponding to the energy change of transferring the QM subsystem from the gas phase into the condensed phase, which is defined by:

$$\Delta E_{qm/mm}(S) = \langle \Psi(S) | H^{o}_{qm}(S) + H_{qm/mm}(S) | \Psi(S) \rangle - E^{o}_{g}(S) \tag{5.28}$$

In eqns (5.25)–(5.28), we have identified the energy terms involving electronic degrees of freedom by E and those purely empirical functions by U, the combination of which is also an empirical potential.

Equation (5.26) is especially useful in that the total energy of a hybrid QM and MM system is separated into two "*independent*" terms – the gas-phase energy and the interaction energy – which can now be evaluated using different QM methods. There is sometimes confusion about the accuracy of applications using semiempirical QM/MM potentials.[72] Equation (5.26) illustrates that there are two issues. The first is the intrinsic performance of the model, *e.g.*, the $E^{o}_{qm}(S)$ term, which is indeed not adequate using semiempirical models and that would require *extremely* high-level QM methods to achieve the desired accuracy. This is only possible by using CCSD(T), CASPT2 or well-tested density functionals along with a large basis set, none of which methods are tractable for applications to enzymes. When semiempirical methods are used, the PES for the $E^{o}_{qm}(S)$ term, is either reparameterised to fit experimental data, or replaced by high-level results. Only in rare occasions when a semiempirical model yields good agreement with experiment, are these methods directly used without alteration.[73,74]

The second issue on accuracy is in the calculation of the $\Delta E_{qm/mm}(S)$ term. It was recognised early on,[65,69,75] when explicit QM/MM simulations were carried out, that combined QM/MM potential is an empirical model, which contains empirical parameters and should be optimised to describe QM/MM interactions. By systematically optimising the associated van der Waals parameters for the "QM-atoms",[65,69,75] both semiempirical and *ab initio* (Hartree–Fock) QM/MM potentials can yield excellent results for hydrogen-bonding and dispersion interactions in comparison with experimental data. The use of semiempirical methods such as the Austin model 1 (AM1)[76] or parameterised model 3

(PM3)[77] in QM/MM simulations has been validated through extensive studies of a variety of properties and molecular systems, including computations of free energies of solvation and polarisation energies of organic compounds,[65,78] the free-energy profiles for organic reactions,[55,73,79] and the effects of solvation on molecular structures and on electronic transitions.[80,81]

The QM/MM PES combines the generality of quantum-mechanical methods for treating chemical processes with the computational efficiency of molecular mechanics for large molecular systems. The use of an explicit electronic-structure method to describe the enzyme-active site is important because understanding the changes in electronic structure along the reaction path can help to design inhibitors and novel catalysts. It is also important because the dynamic fluctuations of the enzyme and aqueous solvent system have a major impact on the polarisation of the species involved in the chemical reaction, which, in turn, affects the chemical reactivity.[65,82] Combined QM/MM methods have been reviewed in several articles.[66–67,83–85,]

5.3.2 The MOVB Potential

A novel combined QM/MM approach has been developed that utilises a mixed molecular-orbital and valence-bond (MOVB) theory to represent the reactive potential-energy surface. In this MOVB approach, molecular orbital theory based on a block-localised orbital scheme is used to define the Lewis resonance structures.[11,86] These Lewis resonance structures are called effective diabatic states, representing the reactant state, the product state or other states important for the transition state of the chemical reaction under investigation, which are coupled by configuration interaction (CI).[12–14] A closely analogous model is the empirical valence bond (EVB) potential that has been used by Warshel and coworkers,[87] who approximate these effective diabatic states by an empirical force field, making the computation cheap for simulation studies. Although it is perfectly reasonable to use empirical force field to represent these diabatic states, provided that the force field is adequately parameterised to reflect the true electronic structure for the entire system, in practice, it is often assumed that the atomic partial charges are invariant by taking values at the reactant state and product state, respectively. This is a major shortcoming because intramolecular charge polarisation is ignored, which leads to inconsistent representation of the bond orders for the ''primary'' and ''secondary'' sites when KIEs are being computed. Note that although it is possible to parameterise the free-energy barrier and its change from water to the enzyme by reproducing experimental results, there is no rigorous justification for the accuracy of the 3N-degree of freedom PES, casting doubt on results that require a knowledge of the gradient and Hessian of the potential surface, a prerequisite for computing KIEs.

Truhlar and coworkers developed a multiconfiguration molecular-mechanics (MCMM) method that involves a systematic parameterisation for the off-diagonal element.[88,89] The MCMM method is fitted to reproduce *ab initio*

energies and gradients. Thus, the MCMM potential as well as the MOVB theory are proper empirical and first-principle functions, respectively, for use in computing nuclear quantum effects and kinetic isotope effects.

5.4 Computational Details

In the path integral simulations using algorithms 1 and 2, we employ a combined QM/MM potential in molecular-dynamics simulations.[65,66] In these studies, the solute is represented explicitly by an electronic-structure method and the solvent is approximated by the three-point charge TIP3P model for water.[90] In the deprotonation of nitroethane by acetate ion, the standard semiempirical AM1 model[76] failed to yield adequate energetic results. Consequently, a set of specific reaction parameters (SRP) has been developed within the AM1 formalism to fit results from high-level *ab initio* theory as well as from experiments.[10,55] The performance of the SRP-AM1 model has been reported previously, and we focus here on the study of the kinetic isotope effects using the PI-FEP/UM method.

In the study of carbon acid deprotonation using the KP2 theory, the solute is treated by B3LYP/6-31 + G(d,p) density functional theory, whereas the solvent is represented by the polarisable continuum model with a dielectric constant of 78 for water. Note that the KP centroid path-integral method is numerical integration free; thus, high-level electronic-structure methods such as DFT with a relatively large basis set can be used. In these calculations, the potential along each normal mode direction for the reactant state, transition state and product state is determined at the B3LYP level by stepping in each direction at an interval of 0.1 Å, and the resulting potential is fitted to a 20th-order polynomial, whose Gaussian smearing integrals (eqn (5.22)) have been derived analytically at the KP2 level. Thus, our results are obtained at the KP2/P20 level for the proton-transfer reactions of a series of aryl-substituted α-methoxystyrene compounds to acetate ion.

For algorithms 1 and 2, the simulations were performed using periodic boundary conditions in the isothermal–isobaric (NPT) ensemble at 25 °C and 1 atm. A total of 898 water molecules were included in a cubic box of about $30 \times 30 \times 30\,\text{Å}^3$. Nonbonded electrostatic interactions are described by the particle-mesh Ewald summation method for QM/MM simulations,[91] whereas van der Waals interactions are smoothed to zero at 9.5 Å based on group–group separations. The bond lengths and angles of solvent water molecules are constrained by the SHAKE algorithm, and an integration step of 1 fs was used for all calculations.[92]

The potential of mean force (PMF) profile is obtained using the umbrella sampling technique.[93] For the proton-transfer reaction between nitroethane and acetate ion, the classical reaction coordinate is defined as the difference in distance for the proton between the donor (α carbon of nitroethane) and the acceptor (an oxygen of the acetate ion) atom: $Z_{\text{PT}} = r(\text{C}_\alpha - \text{H}) - r(\text{H} - \text{O})$. A total of *ca.* 4 ns of simulations were performed (with time step of 1 fs).

The BQCP simulations employed 29 168 classical configurations for each isotope (^{1}H, ^{2}H, and ^{3}H; or H, D, and T), combined with 10 path-integral steps per classical step. For the deprotonation reaction the nitroethane Cα-atom, the abstracting acetate oxygen, the transferring proton, as well as the secondary hydrogen atom, are quantised. Each quantised atom has spawned into 32 beads.

To estimate statistical uncertainties in the computed KIEs, the entire path integral simulations have been divided into ten segments, each of which is treated as independent simulations. Standard uncertainties ($\pm 1\sigma$) were determined from the total average and those from the ten separate blocks. All simulations employed the CHARMM program[94] and all path-integral simulations used a parallel version that efficiently distributes integral calculations for the quantised beads.[8–10]

5.5 Illustrative Examples

5.5.1 Proton Transfer between Nitroethane and Acetate Ion

The proton-abstraction reaction of nitroalkane by acetate ion is a classical example, exhibiting an unusual Brønsted relationship in water, known as the nitroalkane anomaly.[95–97] This process is also catalysed by the nitroalkane oxidase in the initial step of the oxidation of nitroalkanes.[98] Valley and Fitzpatrick reported a KIE of 9.2 ± 0.4 for the di-deuterated substrate (1,1-$^2H_2$) nitroethane in nitroalkane oxidase, and 7.8 ± 0.1 for uncatalysed reaction by an acetate ion in water.[99] We have previously studied the solvent effects and reported preliminary results of H/D kinetic isotope effects.[55] Then, the KIEs for all D and T primary and secondary isotope effects were determined.[32]

The computed PMF, in which the "primary" and "secondary" hydrogen atoms as well as the donor carbon and acceptor oxygen atoms are quantised for the deprotonation of nitroethane by acetate, reveals a computed barrier of 24.4 kcal/mol,[10,32,55] in reasonable accord with the experimental values of 24.8.[99] Without the quantum contribution the computed barrier would have been 27.4 kcal/mol, illustrating the importance of including nuclear quantum effects to accurately determine the free energy of activation for proton-transfer reactions.[100]

The computed primary and secondary KIEs for D and T substitutions are listed in Table 5.1. Figure 5.1 depicts an illustrative example of the computed ratio of the partial quantum partition functions as a function of the centroid path integral reaction coordinate. The kinetic isotope effects have been computed without including the free-energy difference given in eqn (5.16), which may introduce some errors in the present calculations. The computed H/D primary and secondary intrinsic KIEs are $k_H^H/k_D^H = 6.63 \pm 0.31$ and $k_H^H/k_H^D = 1.34 \pm 0.13$, respectively, whereas the total effect where both primary and secondary hydrogen atoms are replaced by a deuterium isotope is $k_H^H/k_D^D = 8.31 \pm 0.13$ (Table 5.1), which may be compared with the

Table 5.1 Computed and experimental primary and secondary kinetic isotope effects for the proton-transfer reaction between nitroethane and acetate ion in water at 25 °C.[a]

KIE	*PI-FEP/UM*	*Expt.*[b]
Primary KIE		
k_H^H/k_D^H	6.63 ± 0.31	
k_H^H/k_T^H	12.96 ± 0.98	
K_D^D/k_T^D	2.17 ± 0.04	
Secondary KIE		
k_H^H/k_H^D	1.340 ± 0.132	
k_H^H/k_H^T	1.375 ± 0.183	
K_D^D/k_D^T	1.096 ± 0.039	
Total KIE		
k_H^H/k_D^D	8.31 ± 0.13	7.8

[a]Kinetic isotope effects are determined by using the average value of the top two bins in the potential of the mean force for the ratio of the partial quantum partition function for the transition state, and the average value of the middle fifteen bins for the reactant state. The bin size used for data collection is 0.05 Å in the reaction coordinate, half of which may be considered as the error in the reaction coordinate value.
[b]Ref. [99].

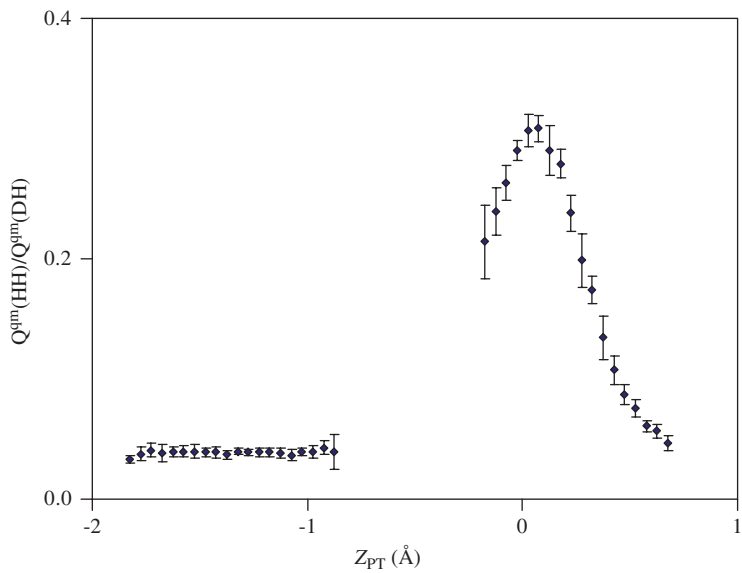

Figure 5.1 Computed ratio of the quantum-mechanical partition functions for the primary H/D kinetic isotope effects in which the secondary site is occupied by a hydrogen along the proton-transfer reaction coordinate. The PI-FEP/UM method was used.

experimental value of 7.8.[99] There are no experimental data for comparison with the results of single-site substitutions.

The computational results allow us to examine the rule of the geometric mean (RGM),[101] which is expressed as follows:

$$k_H^H/k_D^H = k_H^D/k_D^D = \frac{(k_H^H/k_D^D)}{(k_H^H/k_H^D)} \tag{5.29}$$

The RGM states that there is no isotope effect from a second site on the kinetic isotope effect of the first site.[102] The rule was originally derived at the high-temperature limit with small quantum tunnelling corrections,[101] and it has been shown to have negligible deviations on model systems using semiclassical transition-state theory.[103] However, deviations or the observations of RGM breakdown are often used as a measure of the extent of tunnelling in the system.[102] Using the RGM of eqn (5.29), we obtain an estimated value of 8.88 (6.63×1.34) for the total deuterium KIE if the free energies of the primary and secondary KIE were additive. This gives a ratio of 1.07 over the actual computed value (8.31). Another way of interpreting the results is that there is a secondary kinetic isotope effect of 1.07 on the primary kinetic isotope effects:

$$g_{HD}^{HD} = \frac{(k_H^H/k_D^H)}{(k_H^D/k_D^D)} = \frac{6.630}{(8.308/1.340)} = 1.07 \tag{5.30}$$

This result indicates that there is some correction in the motions between the secondary hydrogen and the primary hydrogen in the proton-transfer reaction between nitroethane and acetate ion in water.

Primary and secondary tritium kinetic isotope effects are also given in Table 5.1, which have values of $k_H^H/k_T^H = 12.96 \pm 0.98$ and $k_H^H/k_H^T = 1.37 \pm 0.18$. These effects are greater than the deuterium KIEs because of its larger mass. Employing the rule of the geometric mean, an estimated total tritium KIE of $k_H^H/k_T^T = 17.8$ is obtained.

The single site Swain–Schaad exponents[104] is expressed below using the notation of Huskey,[102]

$$n_{HD} = \frac{\ln(k_H^H/k_T^H)}{\ln(k_H^H/k_D^H)} \tag{5.31}$$

and

$$n_{DT} = \frac{\ln(k_H^H/k_T^H)}{\ln(k_D^H/k_T^H)} \tag{5.32}$$

These equations assume that the isotope effects are determined solely by the use of a one-frequency model with contributions only from the zero-point energy without tunnelling. Studies have shown that the value of n_{HD} for primary KIEs is typically in the range of 1.43–1.45.[102] Deviations from these values are

thought to be indications of contributions from tunnelling.[105] Using the data in Table 5.1, we obtained a single-site Swain–Schaad exponent of $n_{HD}^{(1)} = 1.35$ for the primary KIE, and of $n_{HD}^{(2)} = 1.09$ for the secondary KIE. The exponents, $n_{DT}^{(1)}$ and $n_{DT}^{(2)}$, for D/T ratios are 3.82 and 12.3, respectively. These values show significant deviations from the semiclassical limits, particularly on secondary KIEs, which can have greater computational errors because of the small free-energy difference. The deviations may be attributed to too large a secondary H/D effect.

Mixed isotopic Swain–Schaad exponent is often used to assess tunnelling:[104]

$$n_{DT}^{DD} = \frac{\ln(k_H^H/k_T^H)}{\ln(k_D^D/k_T^D)} \tag{5.33}$$

and

$$n_{DD}^{DT} = \frac{\ln(k_H^H/k_H^T)}{\ln(k_D^D/k_D^T)} \tag{5.34}$$

The first equation is the primary Swain–Schaad exponent, which describes the relationship between H/T primary KIE when the secondary position is occupied by a hydrogen atom with the D/T primary KIE when the secondary position is occupied by a deuterium isotope. The second equation describes a similar relationship for the secondary kinetic isotope effects. Values of the mixed Swain–Schaad exponents significantly greater than 3.3 are typically attributed to contributions from tunnelling,[105] and experimental studies showed that the secondary exponent is more sensitive than the primary exponent in this type of analysis.

For the proton-transfer reaction between nitroethane and acetate ion in water, we obtain a primary KIE Swain–Schaad exponent of $n_{DT}^{DD} = 3.31$ and a secondary exponent of $n_{DT}^{DD} = 3.47$. These results are close to the semiclassical limit, suggesting that tunnelling contributions are not significant for this reaction in aqueous solution. It will be interesting to examine the effects of the enzyme-active site on tunnelling and the Swain–Schaad exponents.[98,99]

5.5.2 The Decarboxylation of N-Methyl Picolinate

The primary and secondary heavy atom kinetic isotope effects for the decarboxylation of N-methyl picolinate have been determined by Rishavy and Cleland.[106] QM/MM simulations were carried out for N-methyl picolinate, treated by the AM1 Hamiltonian, in a cubic box ($30 \times 30 \times 30$ Å^3) of 888 water molecules, described by the TIP3P potential.[10] As usual, long-range electrostatic interactions were treated by the PME method for QM/MM potentials.[91] 2 ns of classical dynamics simulations were performed followed by path integral PI-FEP/UM simulations, employing a total of 97 800 classical configurations

for each isotope (^{12}C, ^{13}C, ^{14}N, and ^{15}N), combined with 10 path-integral steps per classical configuration. Each quantised atom was described by 32 beads.

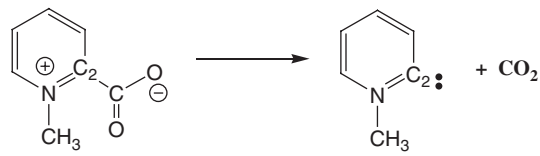

Solvent effects are significant, increasing the free-energy barrier by 15.2 kcal/mol to a value of 26.8 kcal/mol, which is accompanied by a net free energy of reaction of 24.7 kcal/mol. The large solvent effect is due to the presence of a positive charge on the pyridine nitrogen, which is annihilated in the decarboxylation reaction.

Both the $^{12}C/^{13}C$ primary KIE and the $^{14}N/^{15}N$ secondary KIE have been determined (Table 5.2), with the immediate adjacent atoms about the isotopic substitution site quantised as well. To our knowledge, we are not aware of any such simulations prior to our work for a condensed-phase reaction with converged secondary heavy isotope effects.[10] This demonstrate the applicability and accuracy of the PI-FEP/UM method.[10] Figures 5.2 and 5.3 depict the difference between the ^{12}C and ^{13}C quantum effects along the reaction path to illustrate the computational sensitivity using algorithem 1 (PI/UM) and algorithem 2 (PI-FEP/UM). First, the nuclear quantum effects are non-negligible even for bond cleavage involving two carbon atoms, which reduce the free-energy barrier by 0.45 kcal/mol (Figure 5.2). The computed intrinsic ^{13}C primary KIE, without including the reactant state quantum free energy term in eqn (5.16), is 1.0345 ± 0.0051 at 25 °C (Table 5.1). To emphasise the sensitivity of the computational result, the computed KIE is equivalent to a free-energy difference of merely 0.0187 kcal/mol, which is feasible by the use of free-energy perturbation/umbrella sampling techniques. For comparison, the experimental value is 1.0281 ± 0.0003 at 25 °C. For the secondary ^{15}N KIE, the PI-FEP/UM simulation yields an average value of 1.0083 ± 0.0026, which may be compared with experiment (1.0070 ± 0.0003).[106] The agreement between theory and experiment is excellent, which provides support for a unimolecular decarboxylation mechanism in this model reaction.

Table 5.2 Computed and experimental primary $^{12}C/^{13}C$ and secondary $^{14}N/^{15}N$ kinetic isotope effects for the decarboxylation of N-methyl picolinate at 25 °C in water.

	$^{12}k/^{13}k$	$^{14}k/^{15}k$
Exp (120 °C)	1.0212 ± 0.0002	1.0053 ± 0.0002
Exp (25 °C)	1.0281 ± 0.0003	1.0070 ± 0.0003
PI/UM	1.035 ± 0.877	1.007 ± 0.886
PI-FEP/UM	1.034 ± 0.005	1.008 ± 0.003

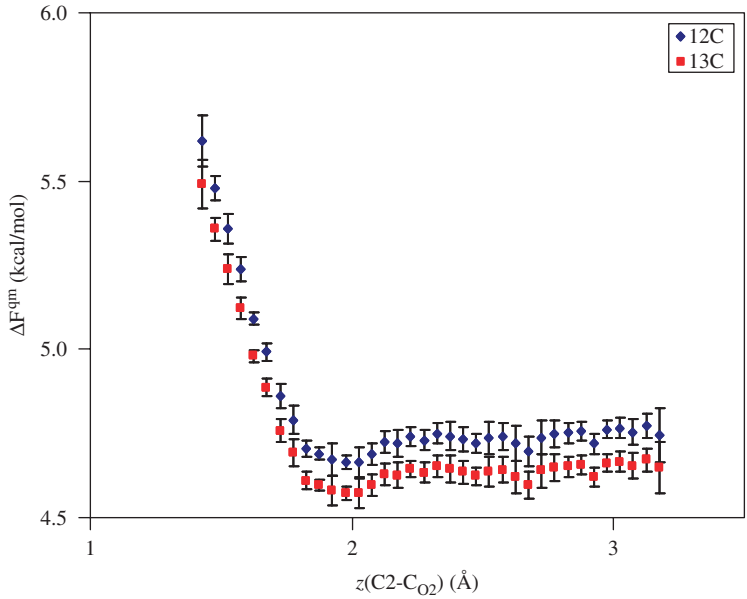

Figure 5.2 Nuclear quantum-mechanical free-energy corrections for the decarboxylation reaction of N-methyl picolinate in aqueous solution from PI/UM calculations. Two separate path integral simulations are performed in this method.

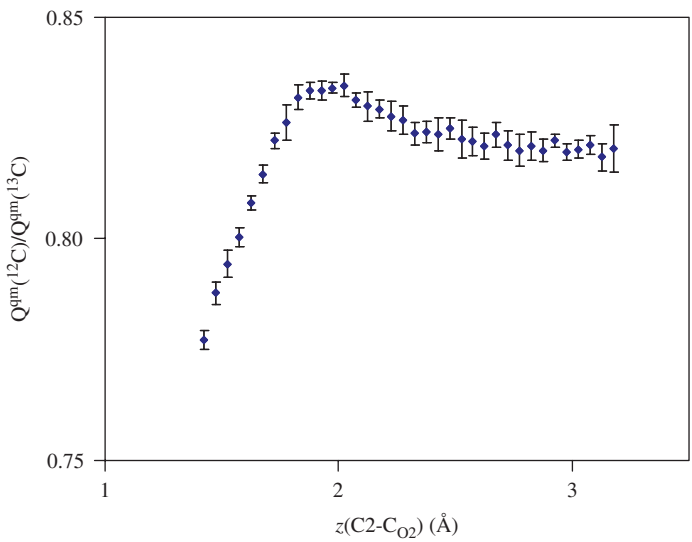

Figure 5.3 The ratio of the quantum-mechanical partition functions between ^{12}C and ^{13}C isotopic substitutions at the carboxyl carbon position from the PI-FEP/UM method. A single path integral simulation was performed.

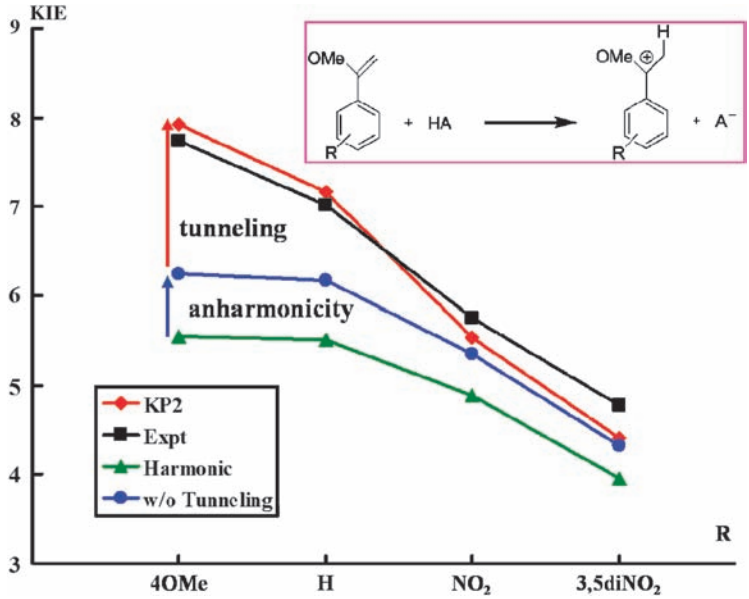

Figure 5.4 Computed primary (protium/deuterium) kinetic isotope effects for the proton-transfer reaction from chloroacetic acid to substituted methoxystyrenes (colour lines) in water represented by a polarizable dielectric continuum model using the KP2/P20 theory (1 = 4-methoxy, 2 = H, 3 = 4-Nitro, and 4 = 3,5-dinitro groups).

5.5.3 Proton Transfer between Chloroacetic Acid and Substituted α-Methoxystyrenes

Richard and coworkers reported the product isotope effects of a series of interesting reactions involving the formation of carbocations from aryl-substituted (R) α-methoxystyrenes by proton transfer from chloroacetic acid.[107,108] These product isotope effects have been converted into KIEs, and the effects of substituents on the observed KIEs have been determined by the KP2/P20 theory.[7] Figure 5.4 shows the computed KIEs using only harmonic frequencies (zero-point energies) and the KP2/P20 values that include tunnelling and anharmonic corrections. Clearly, although the harmonic values correctly reproduced the experimental trend as a function of substituent electron-withdrawing power, the absolute values are significantly underestimated in comparison with experiment. Inclusion of anharmonicity for the description of the individual potential along each normal mode coordinate and tunnelling near the barrier top is critical to obtaining quantitative results for the computed KIEs.

5.6 Concluding Remarks

Centroid path integral methods have been presented for computing kinetic isotope effects for chemical reactions in aqueous solution. Three algorithms are

described: the first two algorithms involve discretised centroid path integral simulations to make quantum corrections to the classical free-energy path, and the third algorithm employs Kleinert variational perturbation theory at the second order in which the path integrals have been integrated analytically. In computing kinetic isotope effects, the first discretised simulation method is similar to the quantised classical path (QCP) approach developed by Hwang and Warshel, but we have developed a fast-converging sampling scheme, namely the bisection sampling method BQCP, by extending the method originally used by Ceperley and coworkers. In the second simulation algorithm, free-energy perturbation is employed by perturbing the light isotope mass into a heavier one in one single simulation, thereby avoiding the need of subtracting two quantum free energies with equally large fluctuations from two separate simulations. Thus, the accuracy in the computed KIEs is significantly improved. In Kleinert variational perturbation theory, analytical results are obtained when the potential surface is represented as a polynomial function, avoiding numerical convergence problems altogether. These methods are illustrated by computing the primary and secondary KIEs, analysing the results of the rule of geometric mean, and elucidating substituents effects. Three reactions have been considered: the proton abstraction of nitroethane by acetate ion, the proton-transfer reaction between substituted methoxystyrenes and chloracetic acid, and the decarboxylation of N-methyl picolinate, all of which are in water.

These examples illustrate the shortcomings of the two-separate simulation strategy of algorithem 1, typically used in the literature in path integral-based calculations of KIEs, and improved accuracy in the integrated centroid path integral–free energy perturbation and umbrella sampling scheme (algorithem 2) that uses a single simulation of a single isotope by perturbing its mass in the context of bisection sampling. Finally, the Kleinert variational perturbation theory gives an automated, numerical integration-free method for computing KIEs. The KP theory has the feature of exponentially and uniformly convergent such that the second-order perturbation (KP2) is sufficient to provide accurate results. An instantaneous normal mode approximation was made to extend the KP2 theory to multidimensional systems.

Acknowledgments

This work has been supported in part by the National Institutes of Health (grant number GM46736) and by a grant from the Office of Naval Research to develop integrated tools for computational chemical dynamics.

References

1. A. Kohen, H. H. Limbach (Eds.) *Isotope Effects in Chemistry and Biology,* Taylor & Francis Group, CRC Press, New York, 2005.
2. J. Pu, J. Gao and D. G. Truhlar, *Chem. Rev.*, 2006, **106**, 3140–3169.
3. J. Gao, S. Ma, D. T. Major, K. Nam, J. Pu and D. G. Truhlar, *Chem. Rev.*, 2006, **106**, 3188–3209.

4. V. L. Schramm, *Acc. Chem. Res.*, 2003, **36**, 588–596.
5. J. Gao and D. G. Truhlar, *Ann. Rev. Phys. Chem.*, 2002, **53**, 467–505.
6. H. Kleinert, *Path Itegrals in Quantum Mechanics, Statistics, Polymer Physics, and Financial Markets*, 3rd edn ed. Singapore, World Scientific; 2004.
7. (a) K.-Y. Wong and J. Gao, *J. Chem. Phys.*, 2007, **127**, 211103. (b) K.-Y. Wong and J. Gao, *J. Chem. Theory Comput.*, 2008, **4**, 1409–1422.
8. D. T. Major and J. Gao, *J. Mol. Graph. Model*, 2005, **24**, 121–127.
9. D. T. Major, M. Garcia-Viloca and J. Gao, *J. Chem. Theory Comput.*, 2006, **2**, 236–245.
10. D. T. Major and J. Gao, *J. Chem. Theory Comput.*, 2007, **3**, 949–960.
11. Y. Mo and J. Gao, *J. Comput. Chem.*, 2000, **21**, 1458–1469.
12. Y. Mo and J. Gao, *J. Phys. Chem. A*, 2000, **104**, 3012–3020.
13. J. Gao and Y. Mo, *Prog. Theor. Chem. Phys.*, 2000, **5**, 247–268.
14. J. Gao, M. Garcia-Viloca, T. D. Poulsen and Y. Mo, *Adv. Phys. Org. Chem.*, 2003, **38**, 161–181.
15. A. Warshel and M. Karplus, *J. Am. Chem. Soc.*, 1972, **94**, 5612–5625.
16. A. Warshel and M. Levitt, *J. Mol. Biol.*, 1976, **103**, 227–249.
17. A. Fernandez-Ramos, J. A. Miller, S. J. Klippenstein and D. G. Truhlar, *Chem. Rev.*, 2006, **106**, 4518–4584.
18. C. Alhambra, J. Gao, J. C. Corchado, J. Villa and D. G. Truhlar, *J. Am. Chem. Soc.*, 1999, **121**, 2253–2258.
19. C. Alhambra, J. Corchado, M. L. Sanchez, M. Garcia-Viloca, J. Gao and D. G. Truhlar, *J. Phys. Chem. B*, 2001, **105**, 11326–11340.
20. D. G. Truhlar, J. Gao, C. Alhambra, M. Garcia-Viloca, J. Corchado, M. L. Sanchez and J. Villa, *Acc. Chem. Res.*, 2002, **35**, 341–349.
21. M. Garcia-Viloca, J. Gao, M. Karplus and D. G. Truhlar, *Science*, 2004, **303**, 186–195.
22. S. Hammes-Schiffer, *Curr. Opin. Struct. Biol.*, 2004, **14**, 192–201.
23. R. P. Feynman and A. R. Hibbs, *Quantum Mechanics and Path Integrals,* McGraw-Hill, New York, 1965.
24. D. Chandler and P. G. Wolynes, *J. Chem. Phys.*, 1981, **74**, 4078–4095.
25. M. Sprik, M. L. Klein and D. Chandler, *Phys. Rev. B*, 1985, **31**, 4234–4244.
26. B. J. Berne and D. Thirumalai, *Ann. Rev. Phys. Chem.*, 1986, **37**, 401–424.
27. G. A. Voth, *Adv. Chem. Phys.*, 1996, **93**, 135–218.
28. N. Chakrabarti, T. Carrington Jr. and B. Roux, *Chem. Phys. Lett.*, 1998, **293**, 209–220.
29. D. Marx, M. E. Tuckerman and G. J. Martyna, *Comp. Phys. Commun.*, 1999, **118**, 166–184.
30. M. E. Tuckerman and D. Marx, *Phys. Rev. Lett.*, 2001, **86**, 4946–4949.
31. M. H. M. Olsson, P. E. M. Siegbahn and A. Warshel, *J. Biol. Inorg. Chem.*, 2004, **9**, 96–99.
32. J. Gao, K.-Y. Wong and D. T. Major, *J. Comput. Chem.*, 2008, **29**, 514–522.
33. J. K. Hwang, Z. T. Chu, A. Yadav and A. Warshel, *J. Phys. Chem.*, 1991, **95**, 8445–8448.

34. J. K. Hwang and A. Warshel, *J. Phys. Chem.*, 1993, **97**, 10053–10058.
35. J.-K. Hwang and A. Warshel, *J. Am. Chem. Soc.*, 1996, **118**, 11745–11751.
36. H. Kleinert, *Phys. Rev. D*, 1998, **57**, 2264.
37. W. Janke and H. Kleinert, *Phys. Rev. Lett*, 1995, **75**, 2787.
38. M. J. Gillan, *Phys. Rev. Lett.*, 1987, **58**, 563–566.
39. G. A. Voth, D. Chandler and W. H. Miller, *J. Chem. Phys.*, 1989, **91**, 7749–7760.
40. J. Cao and G. A. Voth, *J. Chem. Phys.*, 1994, **101**, 6184–6192.
41. J. N. Gehlen, D. Chandler, H. J. Kim and J. T. Hynes, *J. Phys. Chem.*, 1992, **96**, 1748–1753.
42. M. Messina, G. K. Schenter and B. C. Garrett, *J. Chem. Phys.*, 1993, **98**, 8525–8536.
43. G. A. Voth, *J. Phys. Chem.*, 1993, **97**, 8365–8377.
44. R. F. Grote and J. T. Hynes, *J. Chem. Phys.*, 1981, **74**, 4465–4475.
45. M. J. Gillan, *Philos. Mag. A*, 1988, **58**, 257–283.
46. D. E. Makarov and M. Topaler, *Phys. Rev. E: Stat. Phys., Plasmas, Fluids, Relat. Interdiscip. Top.*, 1995, **52**, 178–188.
47. M. Messina, G. K. Schenter and B. C. Garrett, *J. Chem. Phys.*, 1995, **103**, 3430–3435.
48. G. Mills, G. K. Schenter, D. E. Makarov and H. Jonsson, *Chem. Phys. Lett.*, 1997, **278**, 91–96.
49. S. Jang, G. A. Voth, *J. Chem. Phys.* 2000, **112**, 8747–8757. Erratum: 2001. **8114**, 1944.
50. I. Feierberg, V. Luzhkov and J. Aqvist, *J. Biol. Chem.*, 2000, **275**, 22657–22662.
51. J. Villa and A. Warshel, *J. Phys. Chem. B*, 2001, **105**, 7887–7907.
52. M. H. M. Olsson, P. E. M. Siegbahn and A. Warshel, *J. Am. Chem. Soc.*, 2004, **126**, 2820–2828.
53. E. L. Pollock and D. M. Ceperley, *Phys. Rev. B*, 1984, **30**, 2555–2568.
54. D. M. Ceperley, *Rev. Mod. Phys.*, 1995, **67**, 279–355.
55. D. T. Major, D. M. York and J. Gao, *J. Am. Chem. Soc.*, 2005, **127**, 16374–16375.
56. D. T. Major and J. Gao, *J. Am. Chem. Soc.*, 2006, **128**, 16345–16357.
57. R. P. Feynman and H. Kleinert, *Phys. Rev. A*, 1986, **34**, 5080.
58. R. Giachetti and V. Tognetti, *Phys. Rev. Lett.*, 1985, **55**, 912.
59. T. D. Hone, J. A. Poulsen, P. J. Rossky and D. E. Manolopoulos, *J. Phys. Chem. B.*, 2008, **112**, 294–300.
60. J. A. Poulsen, G. Nyman and P. J. Rossky, *J. Chem. Theory Comput.*, 2006, **2**, 1482–1491.
61. B. Palmieri and D. Ronis, *Phys. Rev. E*, 2006, **74**, 061105.
62. D. F. Coker, S. Bonella, *Springer Series in Chemical Physics*, 2007, **83**, 321.
63. A. D. MacKerell Jr., D. Bashford, M. Bellott, R. L. Dunbrack, J. D. Evanseck, M. J. Field, S. Fischer, J. Gao, H. Guo, S. Ha, *et al.*: *J. Phys. Chem. B* 1998, **102**, 3586–3616.
64. J. W. Ponder and D. A. Case, *Adv. Protein Chem.*, 2003, **66**, 27–85.

65. J. Gao and X. Xia, *Science*, 1992, **258**, 631–635.
66. J. Gao, in *Rev. Comput. Chem.* ed. K. B. Lipkowitz, D. B. Boyd: VCH, 1995, 119–185. **vol 7**.
67. M. J. Field, P. Bash and A. M. Karplus, *J. Comput. Chem.*, 1990, **11**, 700–733.
68. J. Gao, *J. Phys. Chem.*, 1992, **96**, 537–540.
69. M. Freindorf and J. Gao, *J. Comput. Chem.*, 1996, **17**, 386–395.
70. I. H. Hillier, *Theochem.*, 1999, **463**, 45–52.
71. P. A. Bash, M. J. Field and M. Karplus, *J. Am. Chem. Soc.*, 1987, **109**, 8092–8094.
72. A. Warshel, *Ann. Rev. Biophys. Biomol. Struct.*, 2003, **32**, 425–443.
73. J. Gao, *J. Am. Chem. Soc.*, 1995, **117**, 8600–8607.
74. N. Wu, Y. Mo, J. Gao and E. F. Pai, *Proc. Natl. Acad. Sci. USA*, 2000, **97**, 2017–2022.
75. J. Gao, *ACS Symp. Ser.*, 1994, **569**, 8–21.
76. M. J. S. Dewar, E. G. Zoebisch, E. F. Healy and J. J. P. Stewart, *J. Am. Chem. Soc.*, 1985, **107**, 3902–3909.
77. J. J. P. Stewart, *J. Comp. Chem.*, 1989, **10**, 209–220.
78. M. Orozco, F. J. Luque, D. Habibollahzadeh and J. Gao, *J. Chem. Phys.*, 1995, **103**, 9112.
79. J. Gao, *Acc. Chem. Res.*, 1996, **29**, 298–305.
80. J. Gao, *J. Am. Chem. Soc.*, 1994, **116**, 9324–9328.
81. J. Gao and K. Byun, *Theor. Chem. Acc.*, 1997, **96**, 151–156.
82. M. Garcia-Viloca, D. G. Truhlar and J. Gao, *J. Mol. Biol.*, 2003, **327**, 549–560.
83. J. Aaqvist, M. Fothergill and A. Warshel, *J. Am. Chem. Soc.*, 1993, **115**, 631–635.
84. J. Gao and M. A. Thompson, *Combined Quantum Mechanical and Molecular Mechanical Methods,* **vol 712**, American Chemical Society, Washington, DC, 1998.
85. A. J. Mulholland, *Theor. Comput. Chem.*, 2001, **9**, 597–653.
86. Y. Mo, Y. Zhang, J. Gao, *J. Am. Chem. Soc.* 1999, **121**, 5737–5742.
87. A. Warshel and R. M. Weiss, *Ann. N. Y. Acad. Sci.*, 1981, **367**, 370–382.
88. Y. Kim, J. C. Corchado, J. Villa, J. Xing and D. G. Truhlar, *J. Chem. Phys.*, 2000, **112**, 2718–2735.
89. T. V. Albu, J. C. Corchado and D. G. Truhlar, *J. Phys. Chem. A*, 2001, **105**, 8465–8487.
90. W. L. Jorgensen, J. Chandrasekhar, J. D. Madura, R. W. Impey and M. L. Klein, *J. Chem. Phys.*, 1983, **79**, 926–935.
91. K. Nam, J. Gao and D. M. York, *J. Chem. Theory Comput.*, 2005, **1**, 2–13.
92. M. P. Allen and D. J. Tildesley, *Computer Simulation of Liquids*, Oxford University Press, Oxford, 1987.
93. J. P. Valleau, G. M. Torrie, in *Modern Theoretical Chemistry,* vol 5, ed. B. J. Berne, Plenum, 1977, 169–194.

94. B. R. Brooks, R. E. Bruccoleri, B. D. Olafson, D. J. States, S. Swaminathan and M. Karplus, *J. Comput. Chem.*, 1983, **4**, 187.
95. C. F. Baernascconi, *Acc. Chem. Res.*, 1992, **25**, 9.
96. F. G. Bordwell and W. J. Boyle Jr., *J. Am. Chem. Soc.*, 1972, **94**, 3907.
97. A. Kresge, *Can. J. Chem.*, 1974, **52**, 1897.
98. M. P. Valley and P. F. Fitzpatrick, *Biochemistry*, 2003, **42**, 5850–5856.
99. M. P. Valley and P. F. Fitzpatrick, *J. Am. Chem. Soc.*, 2004, **126**, 6244–6245.
100. M. Garcia-Viloca, C. Alhambra, D. G. Truhlar and J. Gao, *J. Chem. Phys.*, 2001, **114**, 9953–9958.
101. J. Bigeleisen, *J. Chem. Phys.*, 1955, **23**, 2264.
102. Huskey, in *Hydrogen-Transfer Reactions*, vol 4, ed. J. T. Hynes, J. P. Klinman, H. H. Limbach, R. L. Schowen, Wiley-VCH Verlag GmbH & Co. KgaA, 2006, 1285.
103. W. H. Saunders Jr, *J. Am. Chem. Soc.*, 1985, **107**, 164–169.
104. C. G. Swain, E. C. Stivers, J. F. Reuwer and L. J. Schaad, *J. Am. Chem. Soc.*, 1958, **80**, 558.
105. Y. Cha, C. J. Murray and J. P. Klinman, *Science*, 1989, **243**, 1325–1330.
106. M. A. Rishavy and W. W. Cleland, *Biochemistry*, 2000, **39**, 4569–4574.
107. W.-Y. Tsang and J. P. Richard, *J. Am. Chem. Soc.*, 2007, **129**, 10330–10331.
108. J. P. Richard and K. B. Williams, *J. Am. Chem. Soc.*, 2007, **129**, 6952–6961.